Talanta 266 (2024) 125119

Contents lists available at ScienceDirect

Talanta

journal homepage: www.elsevier.com/locate/talanta

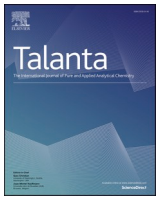

Towards new fluorometric methodologies based on the in-situ generation of gold nanoclusters

Jesús Navarro [a,1], Gemma Cepriá [b,2], Javier Camacho-Aguayo [a], Santiago Martín [c], Alejandro González Orive [d], Susana de Marcos [a,1], Javier Galbán [a,*,1]

[a] Analytical Biosensors Group (GBA), Analytical Chemistry Department, Faculty of Sciences, Instituto de Nanociencia y Materiales de Aragón (INMA), University of Zaragoza-CSIC, C/Pedro Cerbuna 12, 50009, Zaragoza, Spain
[b] Group of Analytical Spectroscopy and Sensors (GEAS), Instituto de Ciencias Ambientales (IUCA), Analytical Chemistry Department, Faculty of Sciences, University of Zaragoza, C/Pedro Cerbuna 12, 50009, Zaragoza, Spain
[c] Instituto de Nanociencia y Materiales de Aragón (INMA), CSIC-Universidad de Zaragoza, Departamento de Química Física, Universidad de Zaragoza, 50009, Zaragoza, Spain
[d] Department of Chemistry, Materials and Nanotechnology Institute, University of La Laguna, Avda. Astrofísico Francisco Sánchez s/n, 38206, San Cristóbal de La Laguna, Spain

ARTICLE INFO

Handling Editor: Joaquim Nobrega

Keywords:
Gold nanoclusters
Fluorescence
Tyramine
In-situ generation
Tuna sample

ABSTRACT

In this manuscript a method for the fluorometric determination of tyramine is described. It is based on the direct reaction between Au(III) and tyramine in a phosphate buffer which produces fluorescent gold nanoclusters (AuNC) (λ_{exc} = 320 nm, λ_{em} = 410 nm) with a diameter of 1.50 ± 0.06 nm. The Au(III) and buffer solutions are mixed and after 140 s, tyramine solution is added; which produces a fast and stable fluorescence signal. The formation of AuNC is demonstrated by STEM and, more importantly, this reaction could be followed by Atomic Fluorescence Microscopy (AFM). The method allows the determination of tyramine in the range from $6.0x10^{-7}$ M (limit of quantification) up to $1.2x10^{-4}$ M; with a relative standard deviation (RSD) ranges from 1.8% to 4.4% depending on the tyramine concentration. The mechanism of AuNC formation involves the Au(III) reduction via the phenol group and the complexation with the amine group. Putrescine and cadaverine do not produce interference, meanwhile histamine causes a proportional decrease in the signal which can be overcome by the standard addition method. The method was applied to the determination of tyramine in a tuna and cheese samples and the results obtained are in statistical agreement with these obtained using a validated or standard method.

1. Introduction

The development of methodologies based on the optical properties of metallic nanomaterials (particularly gold) is one of the fields of analytical nanotechnology in which research is still ongoing. Most of the methodologies have been recently reviewed by different authors [1–3] who state that most of these developments are based on using preformed nanomaterials (nanoparticles) as reagents and determining the analyte on the basis of the changes the nanomaterials suffer, either directly or assisted by additional (bio)chemical reactions (e.g. using enzymes, antibodies, Molecularly Imprinted Polymers -MIP-, etc). The most common methodologies are based on seed-growth, etching, aggregation (coupling) and chemi/physisorption.

A less common alternative method is the in-situ generation of nanomaterials by the analyte; being the starting point the metal ion (M^{n+}). During the process, the ion is reduced to the elemental state (M^0) and, by means of a suitable medium, stabilized as a nanomaterial. These nanomaterials have been used mainly for the analysis of enzymes [3], although there are some cases in which the reductive properties of the analyte have been used for their determination, as is the case of polyphenols [4] or some sugars (in a very basic medium) [5], which can reduce Au(III) to AuNP in the presence of a coating agent.

Tyramine (Tym) is one of the biogenic amines (BA) most frequently found in foods. It is often accompanied by histamine (His), cadaverine

* Corresponding author.
E-mail address: jgalban@unizar.es (J. Galbán).
[1] J. Navarro, S. de Marcos and J. Galbán would like to dedicate this work in memory of Gemma Cepriá for her friendship, enthusiasm and dedication.
[2] deceased.

https://doi.org/10.1016/j.talanta.2023.125119
Received 18 April 2023; Received in revised form 16 August 2023; Accepted 23 August 2023
Available online 24 August 2023

and putrescine. Despite the beneficial functions of Tym in the human body (it is a neurotransmitter [6] and has immunological effects [7]), when ingested in high quantities it can cause some adverse effects, ranging from intolerance to intoxication. The clinical picture produced is known as the "cheese reaction". For this reason, the EFSA (European Food Safety Association) [8] considers Tym and His to be the most potentially toxic, especially in fermented products. The EFSA has called for additional studies to establish the NOAEL (no observed adverse effect level) for Tym and considers 600 mg/day as the toxicological threshold for this BA. For these reasons, rapid methods for the determination of Tym in food extracts are required.

The determination of Tym in food, together with other BAs, is usually performed by HPLC, using detection by UV–visible molecular absorption spectrophotometry (with or without derivatization), fluorescence (with derivatization) [9–11] or mass spectrometry (MS) [12], resulting in a very good sensitivity and selectivity. However, to perform rapid determinations, methods based on the use of solid supports (cellulose type) in combination with fluorescent reagents or nanomaterials have been developed. These methods give good sensitivity (quantification limits between 0.1 and 30 mg Tym/kg sample), with response times, in most cases, above 20 min (up to several hours) [13–19] (see Table S1). The main advantage of the proposed method being the simplicity (no enzymatic reaction is needed), the specificity to other BAs and the fast response (only 140 s).

Our group has developed colorimetric methods for the determination of Tym and other substrates [20] based on the generation of gold nanoparticles [21,22] (or other nanomaterials [23]) and the measurement of its optical properties, by coupling a previous enzymatic oxidation of tyramine with O_2 catalyzed by tyramine oxidase (TAO) [24]. Here, an alternative methodology for the development of rapid methods based on the in-situ and direct generation (without coupling any other type of reaction) of gold nanoclusters is presented. The determination of Tym is used as a proof of concept as it is an analyte for which previous methodologies have been used, making the comparison more efficient.

2. Experimental section

2.1. Reagents

All chemicals were supplied by Sigma Aldrich and used without further purification: Na_2HPO_4 (S9763) and NaH_2PO_4 (S9638) for the buffer preparation, gold chloride hydrate solid (254169) (which was dissolved in Mili-Q water to give a 50 mM solution), tyramine (80345), putrescine (51799), cadaverine (33211) and histamine (59964). Tyramine oxidase (TAO) (EC 1.4.3.6) was obtained from Sekisui Diagnosis with an activity of 4.6 U mg^{-1}.

2.2. Equipment

Fluorescence measurements were carried out mainly using a Photon Technology International (PTI) Time Master fluorescence spectrometer (TM-272003) or a Cay Eclipse fluorescence spectrophotometer (Agilent Technologies). One-centimeter quartz cuvettes were used in all cases. Instrumental conditions are indicated throughout the paper.

A Tecnai F30 (FEI) electronic microscope capable of operating in both scanning and transmission modes was used for acquiring the STEM images and X-ray emission spectra.

Atomic Force Microscopy (AFM) imaging was carried out using a Bruker ICON microscope equipped with a Nanoscope V control unit from Bruker using Peak-Force Tapping mode. AFM data were collected in liquid (10 mM or 0.25 M PBS aqueous solution) using ScanAsyst-Fluid (100−200 kHz and 0.7 N/m, from Bruker) probes. Images were typically recorded with scan rates of 1 Hz/line, 256 lines, and force range of 0.2–2 nN. The time required to complete a 256 × 256-line AFM image is ca. 4 min. Individual spring constants were calibrated using the equipartition theorem, thermal noise procedure [25] while the tip radii were determined by deconvoluting the tip shape after scanning a titanium roughness standard (Bruker) using the Nanoscope off-line v. 1.50 software [26]. In order to minimize tip convolution effects affecting the particle width, data obtained from AFM image profiling have been corrected according to Canet-Ferrer et al. [27]. For the statistical evaluation of the size and height of the NPs, cross-sectional profiling and the Grain Analysis Tool of Gwyddion v. 2.59 package software were applied to isolated NPs from AFM images taken in at least two different, but equivalent, samples.

Cyclic voltammetry measurements were performed with a micro-Autolab FRA2 Type III (Methrom®) potentiostat controlled by NOVA (v 2.1.4) software. A microcrystalline Pt working electrode, a Ag/AgCl/NaCl 3 M reference electrode and a Pt auxiliar electrode were used at a 20 mV/s scan rate.

2.3. Sample treatment

2.3.1. Tuna sample

The sample was prepared and treated by the *Laboratorio de Salud Pública de Aragón* (LSPA). The tuna sample was subjected to acid treatment according to a previously validated method [28]. In short, 2.5 g of tuna were treated with 20 mL 5% trichloroacetic acid; the sample was vortexed for 30 s. The mixture was then subjected to ultracentrifugation for 10 min at 4000 rpm (4 °C). This operation was repeated twice. The filtrate was made up to 50 mL with 5% trichloroacetic acid. The tyramine content was analyzed by HPLC-MS.

2.3.2. Cheese sample

Ten grams of cured cheese were weighed (with ±0.01 precision) and leached with 30 mL 5% trichloroacetic acid for 30 min. Then, the mixture was centrifugated (20 min, 4 °C, 5000 rpm), the solid phase was discarded, and the supernatant solution was neutralized with NaOH (2 M). Next, a second centrifugation was done in the same conditions, and the supernatant was double filtered: firstly, through a 25 mm diameter nylon membrane filter (ALBET-NY-045-25-BL) and secondly, through a 10 kDa centrifugal filter. Finally, the solution was adjusted to 50 mL with 0.1 M pH 7 phosphate buffer.

2.4. Procedure

In the measuring cuvette, 960 μL of phosphate buffer (0.1 M, pH = 8) and 40 μL of Au(III) solution (50 mM) were mixed and immediately the fluorescence intensity was registered (λ_{exc} = 320 nm, λ_{em} = 410 nm). After 140 s, 1 mL of the tyramine or the sample solution were added and the fluorescence signal registered 50 s after the injection.

3. Results and discussion

3.1. Gold nanocluster formation and characterization

Albumin is able to generate gold nanoclusters (AuNC) [29] through a mechanism involving Au(III) reduction by amino acids such as tyrosine and tryptophan (normal reduction potentials below 1V [30]) and the subsequent stabilization of the nanomaterial by the protein. This process requires a basic medium and long reaction times. As the reducing power of tyramine (Tym) is similar to that of tyrosine [31], we hypothesized that it could be used to accelerate the Au(III) reduction by albumin and this could be used to develop a method for Tym determination. Several previous assays were performed under different experimental conditions. Nevertheless, the effect of the albumin concentration was in the opposite direction as expected; the highest fluorescence signal was obtained without albumin (Fig. S1). Fig. 1 shows a 3D fluorescence spectrum obtained during the reaction. As it can be seen, the fluorophore formed has an excitation maximum at 320 nm and an emission maximum at 420 nm.

Therefore, several assays were carried out to confirm that AuNC were

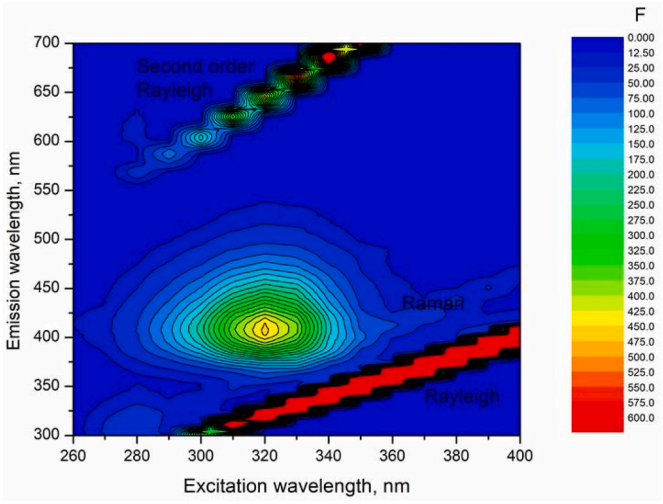

Fig. 1. AuNC 3D fluorescence spectra. Experimental conditions: [Tyramine] = 10^{-5} M, [Au(III)] = 10^{-3} M, pH = 8 (0.1 M, phosphate buffer). Instrumental conditions: 10 nm excitation and fluorescence monochromators spectral bandwidth; 650 V photomultiplier voltage.

indeed formed and, that the observed fluorescence was due to these structures. Fig. 2 shows a STEM image obtained after reacting Tym and Au(III) in a phosphate buffer. As can be seen, small AuNC are formed and located on a bigger spherical particle, attributed to the phosphate buffer (Fig. S2 shows the corresponding X-ray spectra). In terms to confirm the AuNC formation, the reaction was followed by atomic force microscopy (AFM). It is noteworthy that a minimum time of 4 min is required to register an AFM image (see 2B section).

Fig. 3 shows AFM images registered at different times. After 4 min once the reaction began, that the AFM image show how AuNC are already formed with an average size of 1.51 ± 0.07 nm. The subsequent images show that the size of these AuNC do not change during the

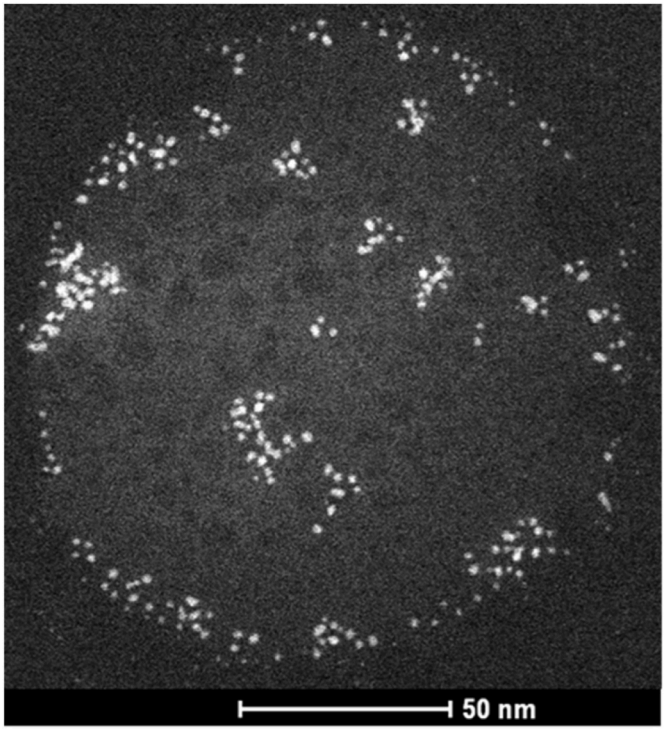

Fig. 2. AuNC STEM image. Experimental Conditions: [Tyramine] = [Au(III)] = 10^{-3} M, pH = 8 (0.1 M, phosphate buffer).

reaction as well as its stability. These results confirm the observations obtained by fluorescence and STEM.

3.2. Optimization and analytical figures of merit

The reaction between Au(III) and Tym requires a capping agent to stabilizes the AuNC. Several authors have demonstrated that different buffers are able to reduce Au(III) and stabilize the formed nanostructures [32]. In our case, the used buffer should not have redox capacity. Several buffers were tested (Tris, carbonate and phosphate) but only phosphate provided good results; since its ability to stabilize nanomaterials [33].

Other aspect to be considered is when the Tym has to be added to the Au(III) in phosphate buffer solution. It has been observed that both the stability and intensity of the fluorescence signal depend on the time interval from Au(III) and phosphate buffer are mixed (t_{mix}) and the Tym solution added. Fig. 4 shows a fluorescence versus time (F = f(t)) plot for different t_{mix}. From this figure, an optimum t_{mix} (140 s) where the fluorescence signal reaches an optimum and stable value is observed. For lower t_{mix}, the fluorescence signal increased rapidly to a maximum (F_{max}) and then decreased. The lower the t_{mix}, the faster the decrease. For higher t_{mix}, albeit the obtained signal is stable, lower F_{max} were reached. Moreover, the longer the t_{mix}, the lower the F_{max}. This behavior was also observed for different Tym concentrations. In addition, the AuNC fluorescence signal was stable up to 15 days.

These F = f(t) representations suggest that the oxidizing capacity of Au(III) depends on the addition time of the phosphate. No information was found in the literature on the complex formation between Au(III) and phosphate and its effect on the reduction ability of Au(III). To gain some information, a voltamperometric study similar to the fluorescence one was carried out, i.e. cyclic voltammograms were recorded at different t_{mix} (Fig. S3). As can be seen, the Au(III) reduction potential (Fig. S3b) in the presence of a phosphate buffer changes with the t_{mix}, decreasing up to a minimum and then recovering. These changes clearly indicate that Au(III) and phosphate form complexes with a slow kinetics which modify the redox capability of Au(III). Fig. 4 and Fig. S3b allow to elucidate the complex with the lowest redox potential gives the most stable fluorescence signal.

The Au(III) concentration and pH of the buffer solution were also optimized (Figs. S4A and S4B). Neither the Au(III) concentration nor the pH affected the optimum t_{mix}, only the intensity of the fluorescence signal.

Under the optimum conditions, the analytical figures of merit were obtained. The linear response range goes from $6.0x10^{-7}$ M (limit of quantification) up to $1.2x10^{-4}$ M. The limit of detection (obtained from $3s_{Bl}$) was $2x10^{-7}$ M. The relative standard deviation (RSD) was obtained for all the calibration points (n = 5) and the values ranged from 4.4% ($6.0x10^{-7}$ M) up to 1.8% ($1.2x10^{-7}$ M). Fig. 5 shows the calibration line (Fluorescence spectra are shown in Fig. S6), where a logarithmic representation has been used for a better visualization.

As shown in Fig. 4, the stability of the AuNC fluorescence signal and the kinetics of the AuNC formation are highly dependent on the t_{mix}. To try to avoid this dependence, a different measurement procedure was tested. In this new method, Tym and phosphate buffer solutions were previously mixed in the cuvette and after that, Au(III) was added. Fig. S5A shows that when a high buffer concentration (ca. 0.25 M) is used, the fluorescence signal appears rapidly and it becomes independent of the t_{mix}. Regarding Au(III), the obtained results show (Fig. S5B) that the lower the Au(III) concentration, the lower but more stable the signal is, so it deserve to give up same sensitivity but get a more reproducible signal. Therefore, when low Au(III) and high buffer concentrations are used, the t_{mix} does not affect the fluorescence signal. Under these conditions, the analytical figures of merit were similar to those obtained previously: linear range from $7.0x10^{-7}$ M (limit of quantification) up to $1.0x10^{-4}$ M. The limit of detection (obtained from $3s_{Bl}$) was $2.5x10^{-7}$ M. The relative standard deviation (RSD) was

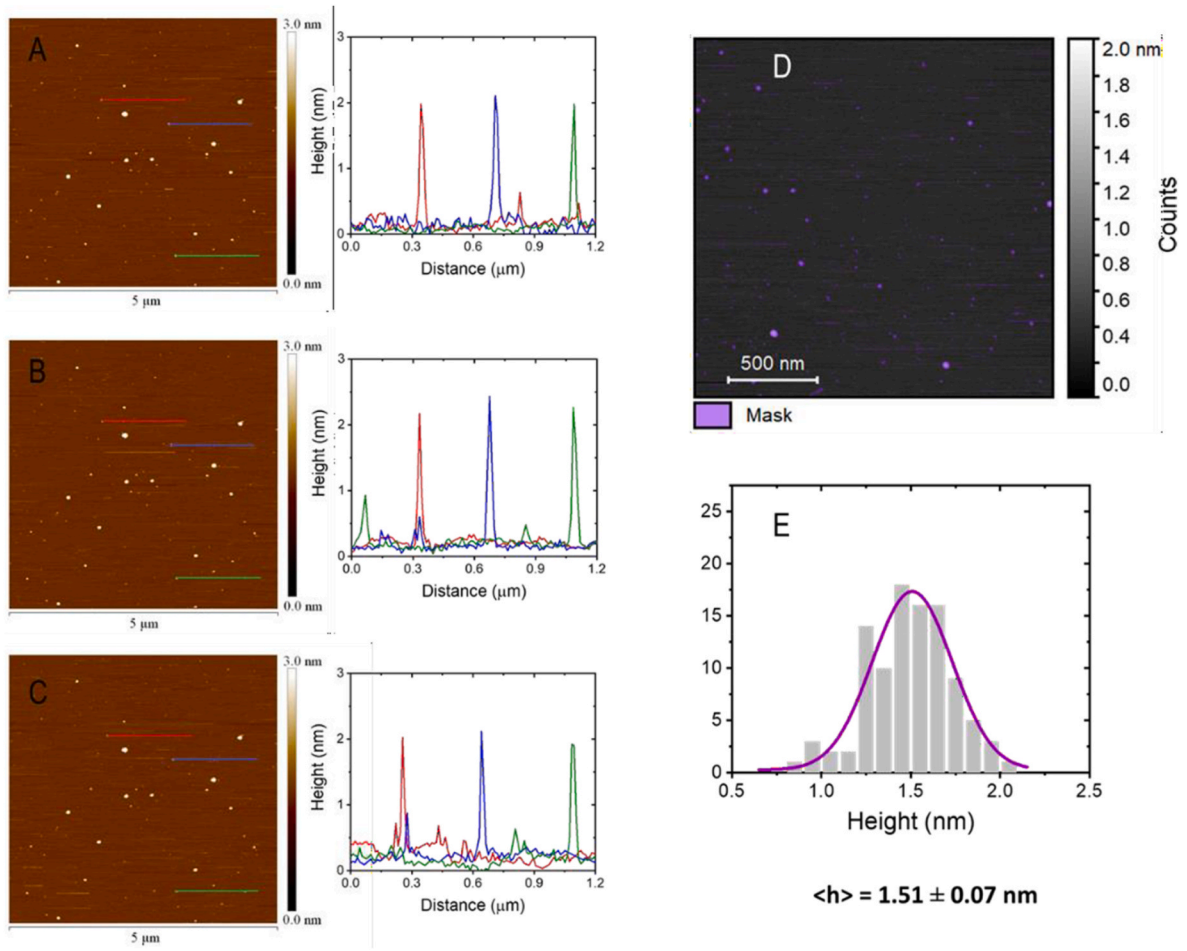

Fig. 3. AFM images obtained during the Tyr/Au(III) reaction. **A**, **B** and **C** correspond to different times from the beginning of the reaction (4, 32 and 100 min, respectively). **D)** Treated image for AuNC height calculation. **E)** AuNC height distribution. Experimental conditions: [Tyramine] = 10^{-3} M), [Au(III)] = 10^{-3} M, pH = 8 (0.1 M, phosphate buffer).

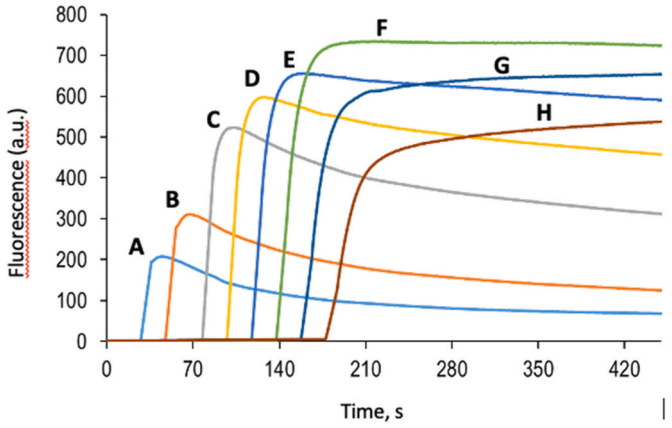

Fig. 4. t_{mix} effect on the AuNC fluorescence signal. Experimental conditions: **A)** 25 s; **B)** 50 s; **C)** 80 s; **D)** 100 s; **E)** 120 s; **F)** 140 s; **G)** 160 s; **H)** 180 s. Experimental conditions: [Tyramine] = 10^{-3} M), [Au(III)] = 10^{-3} M, pH = 8 (0.1 M, phosphate buffer). Instrumental conditions: λ_{exc} = 320 nm; λ_{em} = 420 nm; 10 nm Excitation and fluorescence monochromators spectral bandwidth. 650 V photomultiplier voltage.

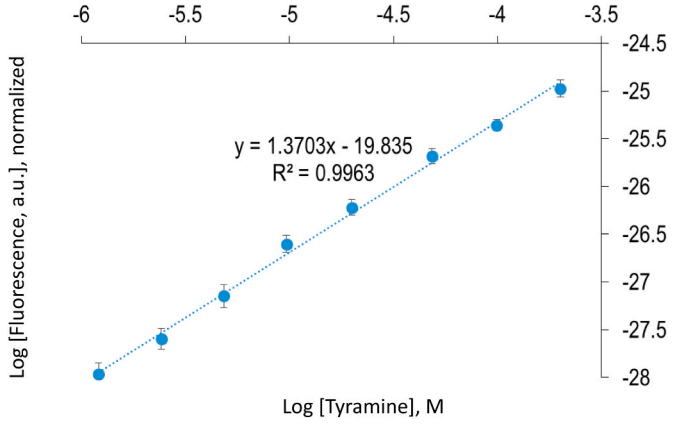

Fig. 5. Tyramine logarithmic calibration line (Fluorescence intensity have been normalized with respect to monochromators spectral) Experimental conditions: [Au(III)] = 10^{-3} M, pH = 8 (0.1 M, phosphate buffer). Instrumental conditions: λ_{exc} = 320 nm; λ_{em} = 420 nm. 650V photomultiplier voltage.

measured for all the calibration points (n = 5) and the values ranged from 4.5% ($6.0x10^{-7}$ M) up to 2.5% ($1.2x10^{-7}$ M). However, the t_{mix} methodology is more recommended, as the required concentration of the phosphate buffer is lower (making the method more prone to interferences from other metal ions) and the Au(III) is higher; which enlarges the linear response range.

3.3. *Mechanism of AuNC formation, interferences and application*

To have information about the reduction mechanism of Au(III) to

AuNcs by Tym will allow to predict what substances could interfere in its determination. In such mechanism, two chemical moieties of the Tym could be involved: the phenolic group (reducing ability) and the amine group (complexing ability). To elucidate this, the ability of other phenolic/amine aromatic compounds to generate fluorescence signals with or without amine groups: phenol, L-tyrosine, serotonin, dopamine and phenylalanine, has been studied. As showed in Table S2, only compounds in which the phenolic group is attached to an amino group (tyrosine and serotonin) show fluorescence signal albeit less intense that for Tym. Phenol also shows a weak signal.

The possible interfering effect of other biogenic amines most frequently found in food (putrescine, cadaverine and histamine (His)) was also evaluated. Putrescine, cadaverine and histamine do not produce fluorescence by themselves (as would be expected, since they are not phenolic compounds). In solutions containing mixtures of Tym with putrescine or cadaverine (up to 10/1 M ratios) no interference was observed; meanwhile His produced a decrease in the Tym signal. The interference level depends on the His/Tym molar ratio (Fig. S7A) and is probably due to the ability of His to complex Au(III), which reduces the amount of Au(III) available to react with Tym (Fig. S7B shows the effect of other His-like compounds). As it can be seen, the signal depressing effect is directly proportional to the histamine concentration, so its interference could be eliminated by the standard addition method. Interfere species such as ions, sugars and reducing agents have also been tested (Fig. S7C), no significative effect was observed in the Tyr signal ($3x10^{-5}$ M) in the presence of these species (in concentration $3x10^{-5}$ M, except Na(I) and K(I) that were 10^{-2} M).

The method here developed, has been applied to determine the presence of Tym in a tuna sample extract. The sample was provided by the LSPA; who previously analyzed the sample using a validated method (see the Experimental section). Fig. S8 compares our calibration line with that obtained by the standard addition method. Although the slope of both lines seems similar they were statistically compared (test-t) and a significant difference was found between them at 95% confidence; this proportional interference is probably due to the presence of His in the sample. The application of the standard addition method gave a Tym content of 281 ± 20 mg/kg in the tuna sample, which was statistically similar (95% confidence level) to that reported by the validated method (HPLC-MS/MS) 302 ± 15 mg/kg [28].

In addition, a sample of cured cheese was also analyzed using the proposed method and the results compared to those obtained with a standard method for the determination of Tym. The standard method is based on the enzymatic reaction of Tym with Tyramine oxidase coupled to a second enzymatic reaction with peroxidase (HRP) and a dye TMB and on the measurement of the $Abs_{650\ nm}$ of the generated TMB_{ox}. In both cases, the sample was analyzed by the standard addition method. The concentration of Tym in the cheese sample, obtained by the proposed method was 265 ± 44 mg/kg, which was statistically similar (95% confidence level) to that obtained by the standard method (240 ± 36 mg/kg). Fig. S9 shows the standard addition calibration plot obtained in each case.

4. Conclusions

The in-situ AuNC generation is a simple and reliable analytical tool for the determination of Tym in real samples. The analytical figures of merit, in terms of limit of quantification, precision, linearity and selectivity are comparable or even better than other previously proposed rapid methods (see Table S1). Additionally, this methodology can be also used for the determination of other compounds as this type of nanostructures can be also formed in other reactions. Future work is focused on exploring new compounds and reactions in terms to expand this methodology.

Credit author statement

Jesús Navarro: Validation; investigation, Gemma Cepriá: investigation (electrochemical experiments); formal analysis, Javier Camacho-Aguayo: Validation, investigation, Santiago Martin: Investigation (AFM experiments); writing; formal analysis, Alejandro Gonzalez Orive: Investigation (AFM experiments); writing; formal analysis, Susana de Marcos: Conceptualization; writing; formal analysis, Javier Galbán: Conceptualization; writing; formal analysis; methodology.

Funding

This work is part of the I + D + i project PID2019-105408 GB-100 supported by MCIN/AEI/10.13039/501100011033 and the funding for research groups pf the Government of Aragon (E25_20R), Spain.

Declaration of competing interest

The authors declare that they have no known competing financial interests or personal relationships that could have appeared to influence the work reported in this paper.

Data availability

No data was used for the research described in the article.

Acknowledgements

The authors would like to acknowledge the Laboratorio de Microscopias Avanzadas-Servicio General de Apoyo a la Investigación (LMA-SAI) of the Universidad de Zaragoza for its technical support. The authors are also very grateful to Dr. Francisco Palacios and Msc Cristina Asensio from the LSPA (DGA) for their valuable help. SM acknowledges DGA/Fondos FEDER (Construyendo Europa desde Aragón) for funding the research group Platón (E31_20R) and also for financial assistance from project LMP154_21.

Appendix A. Supplementary data

Supplementary data to this article can be found online at https://doi.org/10.1016/j.talanta.2023.125119.

References

[1] S. Komal, S. Kukreti, M. Kaushik, Gold nanoclusters: an ultrasmall platform for multifaceted applications, Talanta 234 (2021), 122623, https://doi.org/10.1016/j.talanta.2021.122623.
[2] G.Z. Tsogas, A.G. Vlessidis, D.L. Giokas, Analyte-mediated formation and growth of nanoparticles for the development of chemical sensors and biosensors, Microchim. Acta 189 (2022) 434, https://doi.org/10.1007/s00604-022-05536-7.
[3] A. Scroccarello, F. Della Pelle, M. Del Carlo, D. Compagnone, Optical plasmonic sensing based on nanomaterials integrated in solid supports. A critical review, Anal. Chim. Acta 1237 (2023), 340594, https://doi.org/10.1016/j.aca.2022.340594.
[4] M. Scampicchio, J. Wang, A.J. Blasco, A.S. Arribas, S. Mannino, A. Escarpa, Nanoparticle-based assays of antioxidant activity, Anal. Chem. 78 (2006) 2060–2063, https://doi.org/10.1021/ac052007a.
[5] A. Scroccarello, F. Della Pelle, L. Neri, P. Pittia, D. Compagnone, Silver and gold nanoparticles based colorimetric assays for the determination of sugars and polyphenols in apples, Food Res. Int. 119 (2019) 359–368, https://doi.org/10.1016/j.foodres.2019.02.006.
[6] E. Makrlík, P. Toman, P. Vanura, R. Rathore, Interaction of protonated tyramine with a hexaarylbenzene-based receptor: extraction and DFT study, J. Mol. Struct. 1047 (2013) 277–281, https://doi.org/10.1016/j.molstruc.2013.04.073.
[7] G. Andersen, P. Marcinek, N. Sulzinger, P. Schieberle, D. Krautwurst, Food sources and biomolecular targets of tyramine, Nutr. Rev. 77 (2019) 107–115, https://doi.org/10.1093/nutrit/nuy036.
[8] EFSA (European Food Safety Authority), SCIENTIFIC OPINION, Scientific Opinion on risk based control of biogenic amine formation in fermented foods. EFSA Panel on Biological Hazards (BIOHAZ), EFSA J. 9 (2011) 2393.
[9] B. Redruello, V. Ladero, I. Cuesta, J.R. Álvarez-Buylla, M.C. Martín, M. Fernández, M.A. Alvarez, A fast, reliable, ultra high performance liquid chromatography

method for the simultaneous determination of amino acids, biogenic amines and ammonium ions in cheese, using diethyl ethoxymethylenemalonate as a derivatising agent, Food Chem. 139 (2013) 1029–1035, https://doi.org/10.1016/j.foodchem.2013.01.071.
[10] R. Preti, M.L. Antonelli, R. Bernacchia, G. Vinci, Fast determination of biogenic amines in beverages by a core-shell particle column, Food Chem. 187 (2015) 555–562, https://doi.org/10.1016/j.foodchem.2015.04.075.
[11] H.K. Mayer, G. Fiechter, E. Fischer, A new ultra-pressure liquid chromatography method for the determination of biogenic amines in cheese, J. Chromatogr., A 1217 (2010) 3251–3325, https://doi.org/10.1016/j.chroma.2009.09.027.
[12] V. Sirocchi, G. Caprioli, M. Ricciutelli, S. Vittori, G. Sagratini, Simultaneous determination of ten underivatized biogenic amines in meat by liquid chromatography-tandem mass spectrometry (HPLC-MS/MS), J. Mass Spectrom. 49 (2014) 819–825, https://doi.org/10.1002/jms.3418.
[13] L. Wang, X.M. Xu, Y.S. Chen, J. Ren, Y.T. Liu, HPTLC-FLD-SERS as a facile and reliable screening tool: exemplarily shown with tyramine in cheese, J. Food Drug Anal. 26 (2018) 688–695, https://doi.org/10.1016/j.jfda.2017.07.007.
[14] C. Schaude, C. Meindl, E. Fröhlich, J. Attard, G.J. Mohr, Developing a sensor layer for the optical detection of amines during food spoilage, Talanta 170 (2017) 481–487, https://doi.org/10.1016/j.talanta.2017.04.029.
[15] N.S. Yurova, A. Danchuk, S.N. Mobarez, N. Wongkaew, T. Rusanova, A. J. Baeumner, A. Duerkop, Functional electrospun nanofibers for multimodal sensitive detection of biogenic amines in food via a simple dipstick assay, Anal. Bioanal. Chem. 410 (2018) 1111–1112, https://doi.org/10.1007/s00216-017-0696-9.
[16] Q. Wang, D. Zhang, A novel fluorescence sensing method based on quantum dot-graphene and a molecular imprinting technique for the detection of tyramine in rice wine, Anal. Methods 10 (2018) 3884–3889, https://doi.org/10.1039/c8ay01117f.
[17] N. Kaur, M. Kaur, S. Chopra, J. Singh, A. Kuwar, N. Singh, Fe(III) conjugated fluorescent organic nanoparticles for ratiometric detection of tyramine in aqueous medium: a novel method to determine food quality, Food Chem. 245 (2018) 1257–1261, https://doi.org/10.1016/j.foodchem.2017.11.097.
[18] D. Qiao, Z. Zhang, L. Wang, W. Sheng, Q. Deng, S. Wang, In-situ preparation of molecularly imprinted fluorescent sensing test strips for on-site detection of tyramine in vinegar, Microchem. J. 160 (2021), 105638, https://doi.org/10.1016/j.microc.2020.105638.
[19] B.I. Salman, Y.F. Hassan, W.E. Eltoukhi, R.E. Saraya, Quantification of tyramine in different types of food using novel green synthesis of ficus carica quantum dots as fluorescent probe, Luminescence 37 (2022) 1259–1266, https://doi.org/10.1002/bio.4291.
[20] J. Camacho-Aguayo, S. de Marcos, V. Mora-Sanz, J. Galbán, Selective generation of gold nanostructures mediated by flavo-enzymes to develop optical biosensors, Biosens. Bioelectron. 215 (2022), 114579, https://doi.org/10.1016/j.bios.2022.114579.
[21] J. Navarro, S. de Marcos, J. Galbán, Colorimetric-enzymatic determination of tyramine by generation of gold nanoparticles, Microchim. Acta 187 (2020) 1–8, https://doi.org/10.1007/s00604-020-4141-y.
[22] J. Camacho-Aguayo, S. de Marcos, C. Felices, J. Galbán, In situ enzymatic generation of Au/Pt nanoparticles as an analytical photometric system: proof of concept determination of tyramine, Microchim. Acta 190 (2023) 114, https://doi.org/10.1007/s00604-023-05698-y.
[23] J. Camacho-Aguayo, S. de Marcos, M. Pericás, J. Galbán, Enzymatically mediated fluorescent copper nanocluster generation for tyramine determination, Anal. Bioanal. Chem. (2023) 2037–2044, https://doi.org/10.1007/s00216-023-04571-4.
[24] M. Domínguez, S. Oliver, R. Garriga, E. Muñoz, V.L. Cebolla, S. de Marcos, J. Galbán, Tectomer-Mediated optical nanosensors for tyramine determination, Sensors 23 (2023) 2524, https://doi.org/10.3390/s23052524.
[25] R. Proksch, T.E. Schäffer, J.P. Cleveland, R.C. Callahan, M.B. Viani, Finite optical spot size and position corrections in thermal spring constant calibration, Nanotechnology 15 (2004) 1344, https://doi.org/10.1088/0957-4484/15/9/039.
[26] J.R. Eskelsen, Y. Qi, S. Schneider-Pollack, S. Schmitt, K.W. Hipps, U. Mazur, Correlating elastic properties and molecular organization of an ionic organic nanostructure, Nanoscale 6 (2014) 316–327, https://doi.org/10.1039/c3nr05047e.
[27] J. Canet-Ferrer, E. Coronado, A. Forment-Aliaga, E. Pinilla-Cienfuegos, Correction of the tip convolution effects in the imaging of nanostructures studied through scanning force microscopy, Nanotechnology 25 (2014), 395703, https://doi.org/10.1088/0957-4484/25/39/395703.
[28] ITE-FQ080-02: Determination of biogenic amines by HPLC-MS/MS , Public Heal. Lab. Gov. Aragon (Spain). https://www.aragon.es/documents/20127/1650151/CARTERA_SERVICIOS_LABORATORIO_DGSP_2022.pdf.
[29] J. Xie, Y. Zheng, J.Y. Ying, Protein-directed synthesis of highly fluorescent gold nanoclusters, J. Am. Chem. Soc. 131 (2009) 888–889, https://doi.org/10.1021/ja806804u.
[30] L. Mahmoudi, R. Kissner, T. Nauser, W.H. Koppenol, Electrode Potentials of l -Tryptophan, l -Tyrosine, 3-Nitro- l -tyrosine, 2,3-Difluoro- l -tyrosine, and 2,3,5-Trifluoro- l -tyrosine, Biochemistry 55 (2016) 2849–2856, https://doi.org/10.1021/acs.biochem.6b00019.
[31] J.J. Warren, J.R. Winkler, H.B. Gray, Redox properties of tyrosine and related molecules, FEBS Lett. 586 (2012) 596–602, https://doi.org/10.1016/j.febslet.2011.12.014.
[32] S.R. Ahmed, S. Oh, R. Baba, H. Zhou, S. Hwang, J. Lee, E.Y. Park, Synthesis of gold nanoparticles with buffer-dependent variations of size and morphology in biological buffers, Nanoscale Res. Lett. 11 (2016) 1–11, https://doi.org/10.1186/s11671-016-1290-3.
[33] K. Liu, Z. He, J.F. Curtin, H.J. Byrne, F. Tian, A novel, rapid, seedless, in situ synthesis method of shape and size controllable gold nanoparticles using phosphates, Sci. Rep. 9 (2019) 7421, https://doi.org/10.1038/s41598-019-43921-0.